Separation Science and Technology
Publication details, including instructions for authors and subscription information:
http://www.informaworld.com/smpp/title~content=t713708471

Separation of Oxygen and Nitrogen by Porous Cyanometallates

B. Zamora[a]; M. Autie[ab]; J. L. Contreras[c]; M. Centeno[a]; E. Reguera[ab]
[a] Centro de Investigación en Ciencia Aplicada y Tecnología Avanzada del IPN, Legaría, México DF, México [b] Instituto de Ciencia y Tecnología de Materiales, Universidad de Habana, la Habana, Cuba [c] Universidad Autónoma Metropolitana, Unidad Azcapotzalco, México, DF, México

Online publication date: 04 March 2010

To cite this Article Zamora, B. , Autie, M. , Contreras, J. L. , Centeno, M. and Reguera, E.(2010) 'Separation of Oxygen and Nitrogen by Porous Cyanometallates', Separation Science and Technology, 45: 5, 692 — 699
To link to this Article: DOI: 10.1080/01496390903571101
URL: http://dx.doi.org/10.1080/01496390903571101

Separation Science and Technology, 45: 692–699, 2010

ISSN: 0149-6395 print/1520-5754 online
DOI: 10.1080/01496390903571101

Taylor & Francis
Taylor & Francis Group

Separation of Oxygen and Nitrogen by Porous Cyanometallates

B. Zamora,[1] M. Autie,[1,2] J. L. Contreras,[3] M. Centeno,[1] and E. Reguera[1,2]

[1]*Centro de Investigación en Ciencia Aplicada y Tecnología Avanzada del IPN, Legaría, México DF, México*

[2]*Instituto de Ciencia y Tecnología de Materiales, Universidad de Habana, la Habana, Cuba*

[3]*Universidad Autónoma Metropolitana, Unidad Azcapotzalco, México, DF, México*

The adsorption-based separation in porous solids takes place through steric, kinetic, or equilibrium effect selectivity. In this contribution the oxygen-nitrogen separation by four porous frameworks representative of cyanometallates was studied by inverse gas chromatography. The following materials were considered: $Cd_3[Co(CN)_6]_2$ (cubic), $Zn_3[Co(CN)_6]_2$ (rhombohedral), $Zn_3K_2[Fe(CN)_6]_2$ (rhombohedral) and $Co[Fe(CN)_5NO]$ (cubic). Chromatographic separation profiles from gases mixtures using columns of these materials were recorded. For columns prepared from rhombohedral zinc hexacyanocolbaltate(III) excellent separation of O_2 and N_2 was observed. Such behavior was attributed to a kinetic-based selectivity related to the size and shape for the pore windows of this material. The porous framework of this zinc phase is formed by ellipsoidal cavities ($12.5 \times 9 \times 8$ Å) communicated by elliptical windows of ~ 5 Å. For $Cd_3[Co(CN)_6]_2$ and $Co[Fe(CN)_5NO]$ also kinetic-based selectivity was observed while for $Zn_3K_2[Fe(CN)_6]_2$ the K^+ ion located close to the cavity windows hinders the porous windows accessibility for nitrogen and oxygen molecules. All the samples to be studied were characterized from X-ray diffraction, infrared spectroscopy, termogravimetric and adsorption data.

Keywords adsorption; air separation; porous solids; prussian blue analogue

INTRODUCTION

The large-scale technologies for oxygen and nitrogen production are based on cryogenic distillation of air. These technologies consume relatively large amount of energy. For small and intermediate scales the separation by adsorption is probably the most attractive alternative, and after cryogenic distillation, it is the most widely used process for air separation, particularly when very high product purity is not required. The separation by adsorption is based on the adsorbent selectivity for a given component in the considered mixture. The adsorption is an exothermic process and it is favored at low temperatures. In consequence, the removal of the adsorbed species (desorption) is an endothermic process and requires a temperature increase. The adsorption equilibrium is reached for equal chemical potential for both adsorbed and gaseous phases. A reduction for the chemical potential in the gaseous phase leads to partial desorption for the adsorbed species. This fact supports the gas separation by pressure swing adsorption (PSA) cycles (1,2). For oxygen-nitrogen separation by adsorption five classes of adsorbent materials are currently used: molecular-sieve zeolites, activated carbons, silica gel, activated alumina, and coordination compounds (3). Several of these materials can be integrated in a given PSA-based technology where a feed dryer stage including the CO_2 removal is always incorporated.

The adsorption-based separation is achieved by at least one of the following mechanisms: steric, kinetic, or equilibrium effect. In the steric mechanism the pass of a given species through the porous framework is determined by its size and shape. Oxygen and nitrogen are both ellipsoidal shape molecules but of slightly different size, 3.46 and 3.64 Å (kinetic diameter), respectively (4). Kinetic separation results from a different diffusivity for the adsorbates that are present in the considered mixture. The diffusivity of a given adsorbate through a porous framework depends on its size and also on the nature and strength for the guest-host interactions. Related to their ellipsoidal shape, nitrogen and oxygen are molecules with permanent quadrupole moment, which, in 10^{-26} esu.cm^2 units, is 1.52 for nitrogen and 0.30 for oxygen (5). Molecules with quadrupole moment interact with an electric field gradient. The interaction will be stronger for nitrogen. The large majority of oxygen-nitrogen adsorption-based separation processes are carried out through the control of the adsorption equilibrium, varying the pressure between two extreme values (PSA) under practically isothermal conditions.

Regarding materials, zeolites and activated carbons are among the most widely used. Zeolites with exchangeable alkaline and alkaline earth metals (groups 1 and 2,

Received 28 July 2009; accepted 29 November 2009.

Address correspondence to E. Reguera, Centro de Investigación en Ciencia Aplicada y Tecnología Avanzada del IPN, Legaría 694, México DF, Mexico. E-mail: ereguera@yahoo.com

respectively) show high selectivity for nitrogen related to its larger quadrupole moment (2). Activated carbons are materials of non-polar surface without possibilities for selectivity according to the electrostatic interaction. In this case the separation takes place through a kinetic selectivity controlled by the size of the pore opening, below 5 Å. In this class of materials for oxygen a higher diffusivity is observed (6).

Coordination compounds have also received certain attention for oxygen-nitrogen separation. Nature has many examples of coordination compounds, particularly in proteins, with the ability for reversible oxygen separation from air, among them hemoglobin. In these compounds the oxygen molecule forms a non-dissociative weak coordination bond at a metal open site; an iron atom in hemoglobin, for instance. From this fact, coordination compounds have been studied as model compounds by the abilities shown by some proteins for oxygen separation, storage, transport, and release. Such compounds also find potential applications for oxygen separation from air in industrial processes (4).

In this contribution we are reporting an inverse gas chromatography (IGC) study on the oxygen-nitrogen separation by four materials which are representative of the porous frameworks found for cyanometallates, particularly: $Cd_3[Co(CN)_6]_2$ (cubic), $Zn_3[Co(CN)_6]_2$ (rhombohedral), $Zn_3K_2[Fe(CN)_6]_2$ (rhombohedral) and $Co[Fe(CN)_5NO]$ (cubic). In the following these compounds will be labeled Cd_3Co_2, Zn_3Co_2-R, $Zn_3K_2Fe_2$, and CoNP, respectively. The best results were obtained for Zn_3Co_2-R, a material free of available coordination sites for the oxygen molecule and with a non-polar surface. The observed high selectivity of this material for oxygen was attributed to a kinetic mechanism. For comparison, some gases mixtures containing H_2 and CH_4 were also considered. All the samples to be studied were characterized from X-ray diffraction (XRD), infrared (IR), adsorption, and thermogravimetry (TG) data. To the best of our knowledge, an analogue study for this family of materials has not been reported before.

EXPERIMENTAL

The materials under study were prepared mixing aqueous hot (60°C) solutions (0.01 M) of $K_3[Co(CN)_6]$, $K_4[Fe(CN)_6]\cdot 3H_2O$ and $Na_2[Fe(CN)_5NO]\cdot 2H_2O$, and of sulfate of the involved metals. The resulting precipitates were aged for 24 h. within the mother liqueur at the precipitation temperature followed by their separation by centrifugation. The solid fraction was repeatedly washed with distilled water to remove all the accompanying ions and then air-dried until constant weight. The nature of the obtained powders was corroborated from IR spectra and XRD powder patterns. The metal atomic ratios in the obtained powders were estimated from X-ray dispersed-energy spectroscopy (EDS) analyses. The powder morphology was studied by scanning electron microscopy (SEM). The materials dehydration and thermal stability were evaluated recording TG curves. All the reagents used were analytical grade from Sigma–Aldrich.

IR spectra were recorded in an FT-IR spectrophotometer (Spectrum One spectrometer, from Perkin Elmer) using the KBr pressed disk technique. XRD powder patterns were obtained with CuKα radiation in an HZG-4 diffractometer (from Carl Zeits) and their evaluation carried out using program Dicvol (7).TG curves were collected from 25 up to 300°C, under a N_2 flow (100 mL/min) using a TA instrument thermo-balance (TGA 2950 model) operated in the high-resolution mode in order to select the most appropriate temperature and heating time to obtain anhydrous samples for the gases separation experiments. The pore volume for the materials under study was calculated from carbon dioxide adsorption isotherms using an ASAP 2020 analyzer. The same equipment was used to obtain N_2 and O_2 adsorption isotherms at 0°C.

The IGC data were recorded with GOW-MAC equipment (550 Series, 69–552 model) and a thermo-conductivity detector (TCD) in the 20–50°C temperature range. As carrier gas, helium and argon were evaluated at a flow rate of 20 mL/min, and input pressure of 2.43 and 2.84 bar, respectively. Cleaned and weighed stainless steel columns from 1 to 2.50 m long and of 2.75 and 5.5 mm inner diameter were packed with the materials to be studied. For CoNp and Cd_3Co_2 a column of 3.5 m was required to obtain well resolved N_2 and O_2 peaks. The materials to be studied were pelletized and then milled to obtain a particle size in the 0.3–0.5 mm range. The packed columns were activated overnight under an argon flow at the dehydration temperature indicated by the TG curve.

The adsorbate net retention volumes, V_n, were calculated according to (8):

$$V_n = JV_f(t_R - t_0)(T_C/T_A)(P_0 - P_w)/P_0 \qquad (1)$$

where J is the James-Martin gas compressibility correction factor, V_f is the gas carrier flow rate at the flowmeter temperature T_f, T_C is the column temperature, T_A is the room temperature ($T_A = T_f$), P_0 is the outlet pressure, P_w is the vapor pressure of water at T_f, t_R is the adsorbate retention time relative to t_0, which is the retention time for an adsorbate with a negligible interaction with the column material.

The differential adsorption heat, Q_{ad}, equal to the enthalpy for the standard adsorbed state, ΔH_d^0 (within the Henry zone) where determined from the slope of $\ln(V_n)$ vs. $1/T_C$ plot according to (8):

$$\Delta H_d^0 = -R\ d(\ln(V_n/V_p))/d(1/T_C) \qquad (2)$$

where R is the universal gas constant, and V_p is the pore volume.

The column separation power ($K_{2,1}$) for two given components (1 and 2) in a gases mixture, was estimated from the peaks resolution ($R_{2,1}$) according to:

$$R_{2,1} = 2(t_{R,2} - t_{R,1})/(w_2 + w_1) \quad (3)$$

where $t_{R,2}$ and $t_{R,1}$ are the corresponding retention time, and w_1, w_2 are the peak widths at the half maximum. The $K_{2,1}$ value was then calculated from:

$$K_{2,1} = R_{2,1} - 1 \quad (4)$$

For $K_{2,1} > 1$ the chromatographic peaks for the considered two components in the gases mixture appear well resolved.

RESULTS AND DISCUSSION

Materials Characterization

The metals atomic ratios found from the EDS analyses agree with the expected formula unit for the studied materials. The structural characterization, the thermal stability, and information on the electronic structure of analogues compositions have already been reported (9–11) and here only a summary of their features is provided. The as-synthesized samples are hydrated solids which lose all the crystal water on heating to form stable anhydrous materials where the free volume of their porous framework is available for the adsorption of small size molecules (Fig. 1). $Zn_3K_2[Fe(CN)_6]_2 \cdot xH_2O$ becomes anhydrous from about 140°C and then remain stable up to 350°C (11), $Co[Fe(CN)_5NO] \cdot xH_2O$ dehydrates at 90°C and decomposes close 200°C (9). $Zn_3[Co(CN)_6]_2 \cdot xH_2O$ and $Cd_3[Co(CN)_6]_2 \cdot xH_2O$ form anhydrous solids on heating from about 60 and 80°C, respectively, and then remain stable up to 300°C. Only for the Zn compound the crystal water removal is accompanied by a structural transformation, from cubic to rhombohedral (R-3c space group). In the rhombohedral phase (Zn_3Co_2-R) the zinc atoms are tetrahedrally coordinated to N ends of the CN groups. Its porous framework is formed by ellipsoidal cavities of about $12.5 \times 9 \times 8$ Å that remain communicated by elliptical windows of ~5 Å (Fig. 2) (10,11).This structure

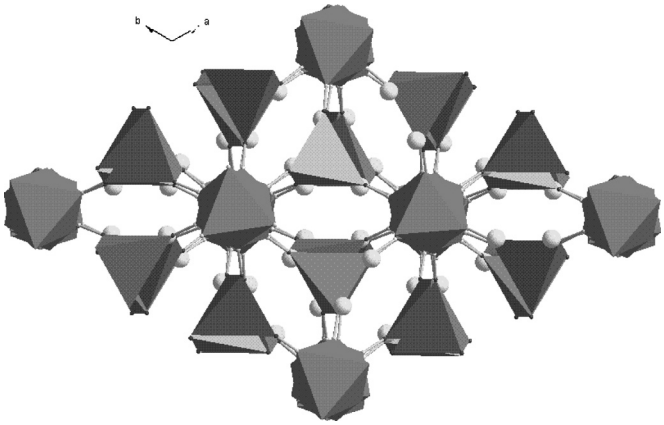

FIG. 2. Porous framework for $Zn_3K_2[Fe(CN)_6]_2$. The small sphere represents the K^+ ions. The rhombohedral phase of $Zn_3[Co(CN)_6]_2$ (Zn_3Co_2-R) has an analogue porous framework but without cations (see Fig. 5, Inset).

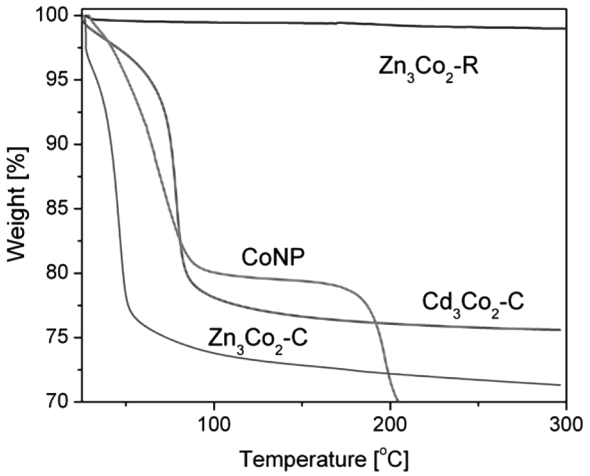

FIG. 1. TG curves for the materials under study. $Co[Fe(CN)_5NO]$ (CoNp) decomposes close to 200°C. On heating cubic $Zn_3[Co(CN)_6]_2$ transforms into the rhombohedral phase (Zn_3Co_2-R), which is an anhydrous material.

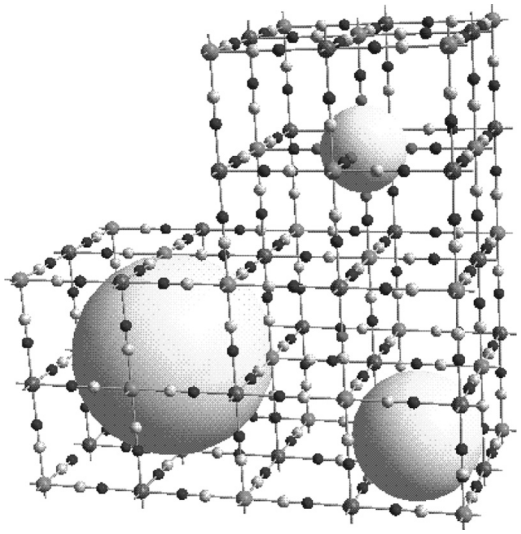

FIG. 3. Porous framework of $Co[Fe(CN)_5NO]$. The larger sphere represents a cavity related to vacancies for the building block, $[Fe(CN)_5NO]$; the sphere of intermediate size indicates the interstitial voids which serve as communication windows, and the smaller one corresponds to a small cavities resulting from vacancies for the Co atom. An analogue porous framework has the porous Prussian blue analogues, e.g. $Cd_3[Co(CN)_6]_2$, but without the smallest cavity.

TABLE 1
Structural parameters and temperature of dehydration and of thermal stability for the materials under study

Material	Unit cell edges (Å)	Space group	Pore volume (cm^3/g)	Dehydration temp. (K)	Stability temp. (K)
CoNP	10.263(1)	Fm3 m	0.37	343	443
Cd_3Co_2	10.591(1)	Pm3 m	0.32	333	>573
Zn_3Co_2-R	a = b = 12.485(1) c = 32.756(1)	R-3c	0.31	—	>573
$Zn_3K_2Fe_2$	a = b = 15.541(1) c = 32.158(1)	R-3c	0.19*	423	>573

*This small value for the pore volume is related to the presence of K^+ ions within the cavities.

can be stabilized at room temperature, even in the presence of water, replacing a small fraction of cobalt atoms by iron (12). $Zn_3K_2Fe_2$ crystallizes with the same rhombohedral unit cell (R-3c space group) where the K^+ atoms are exchangeable species located within the cavities, close to the windows (Fig. 2). Cd_3Co_2 and CoNP crystallize with a cubic unit cell where the cell edge corresponds to the Cd-N≡C-Co-C≡N-Cd (Co-N≡C-Fe-C≡N-Co) chain length. Their porous framework is formed by systematic vacancies of the building block, $[Co(CN)_6]$ and $[Fe(CN)_5NO]$, respectively, to form a network of cavities of *c.a.* 8.5 Å diameter communicated by interstitial free spaces of about 4.5 Å (Fig. 3).At the surface of cavities, six metal centers (Cd, Co) with an unsaturated coordination environment are found. For CoNP the porous framework also contains a system of smaller cavities (~4 Å diameter) related to the non-ability of the NO group to form a coordination bond at its O end with the cobalt atom.

The pore accessibility, pore volume and adsorption potential for the materials under study have been reported from CO_2, H_2O, H_2 and Xe adsorption data (9,10,12–17). For $Zn_3K_2Fe_2$ the exchangeable metal (K) located close to the pore window (Fig. 2) determines the cavity adsorption potential but at the same time limits the pore accessibility for a big adsorbate like Xe but not for CO_2, H_2O and H_2. Table 1 summarizes the structural properties for the considered porous cyanometallates, including their pore volume, and temperatures of dehydration and of thermal stability.

NITROGEN AND OXYGEN ADSORPTION UNDER EQUILIBRIUM CONDITIONS

Figures 4 and 5 show the recorded N_2 and O_2 adsorption isotherms at 0°C for CoNP, Cd_3Co_2, and Zn_3Co_2-R. All these isotherms show a linear dependence on the pressure. Such behavior corresponds to Henry type isotherms (very low coverage) where the isotherm slope senses the strength for the guest-host interaction (adsorption potential). From this fact, the stronger adsorption potential was found for O_2 in CoNP and Cd_3Co_2. This selectivity between O_2 and N_2 cannot be attributed to the electrostatic interaction between the adsorbate quadrupole moment (Q) and the cavity electric field gradient (∇E). Of these two adsorbates, the larger Q value corresponds to N_2, 1.52 vs. 0.30 for O_2, in 10^{-26} esu · cm^2 units. From this fact, the stronger electrostatic guest-host interaction would be expected for nitrogen, which is not observed. At the cavity surface of these two materials six metal centers with an unsaturated coordination environment are found, which are available for a coordination interaction with the oxygen molecule. As already mentioned, the high selectivity of some transition-metal containing compounds for oxygen, among them hemoglobin, is based on the formation of a weak coordination bond with metal centers (4). From these considerations, the stronger guest-host interaction for O_2 in CoNP and Cd_3Co_2 was attributed to the formation of a weak coordination interaction with the metal centers found at the surface of cavities. For Zn_3Co_2-R where the Zn atom has no available coordination sites, practically the same

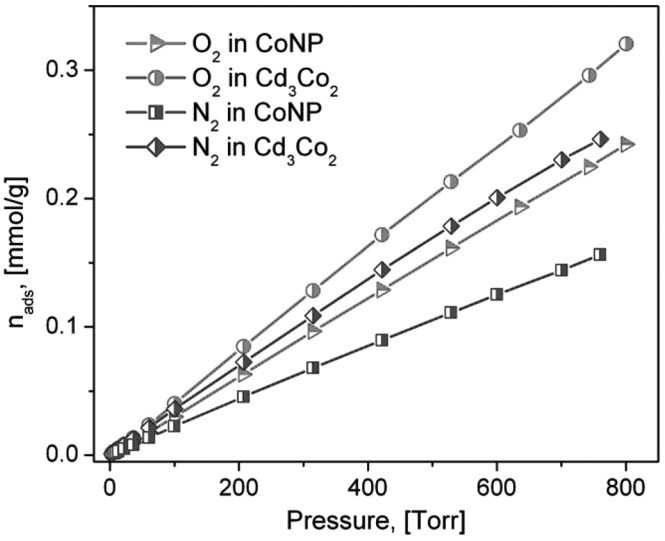

FIG. 4. Nitrogen and oxygen adsorption isotherms for $Co[Fe(CN)_5NO]$ and $Cd_3[Co(CN)_6]_2$ at 0°C.

adsorption isotherms for N_2 and O_2 were obtained (Fig. 5). In addition, this material has a practically non-polar surface, as reveals its anhydrous character even in the presence of humid air (10–12), and the electrostatic interaction with N_2 and O_2 must be very weak. From the adsorption data under equilibrium conditions no selectivity of this material for N_2 or O_2 would be expected.

When the adsorption isotherms slopes for CoNP and Cd_3Co_2 are compared, for both N_2 and O_2 the stronger guest-host interaction is observed for CoNP. To this behavior two factors could be contributing: a greater contribution of dispersive forces related to a slightly smaller cavity size for CoNp respect to Cd_3Co_2 because of the strong π-back bonding effect of the NO group (9); and also a higher coordination ability for Co because of the availability of partially filled 3d orbitals.

For $Zn_3K_2Fe_2$ no adsorption of N_2 or O_2 was observed. This was attributed to a reduction of the effective cavity window size by the presence of K^+ close to the windows limiting the pore accessibility for these two molecules. To that behavior also a relatively strong guest-host electrostatic interaction with the K^+ ion, an effect observed in zeolites (discussed below), could be contributing. The inaccessibility for the free volume of $Zn_3K_2Fe_2$ has also been observed for the Xe adsorption (13). The Xe atom has a kinetic diameter of 4.1 Å, slightly larger than N_2 (3.67 Å), but Xe has no quadrupole moment. The porous framework of this material and of its analogues containing Na, Rb or Cs instead K, is accessible to CO_2(14,17), which has a small cross section along the O-C-O axis, and also to H_2 with a kinetic diameter of 2.9 Å. However, for the analogue containing Na pronounced kinetic effects for the H_2 adsorption are observed, which have been ascribed to a strong electrostatic interaction between this molecule with the Na^+ atom found close to the cavity windows (14).

NITROGEN AND OXYGEN SEPARATION EVALUATED FROM IGC DATA

As reference material for oxygen-nitrogen separation studies from IGC data a column packed with Zeolite 13X was used. Figure 6 shows the recorded chromatographic profile for a mixture of O_2, N_2, and H_2 in that column. Hydrogen was incorporated to the gases mixture as reference for the retention time because for this adsorbate a weak guest-host interaction is expected. The larger retention time was observed for N_2, which was attributed to a stronger electrostatic interaction between the electric field gradient created by the exchangeable metals within the cavity with the adsorbate quadrupole moment. In that Fig. 6. also the chromatographic profile for the same gases mixture and under the same experimental conditions but for the column of Zn_3Co_2-R is shown. The peaks corresponding to the components in the mixture appear well resolved, but for O_2 and N_2 their positions appear inverted relative to the results obtained from the zeolite column. The larger retention time corresponds to O_2, and not to N_2. This behavior was ascribed to a kinetic separation mechanism related to a different diffusivity for O_2 and N_2. Compared with nitrogen, oxygen atom has a greater

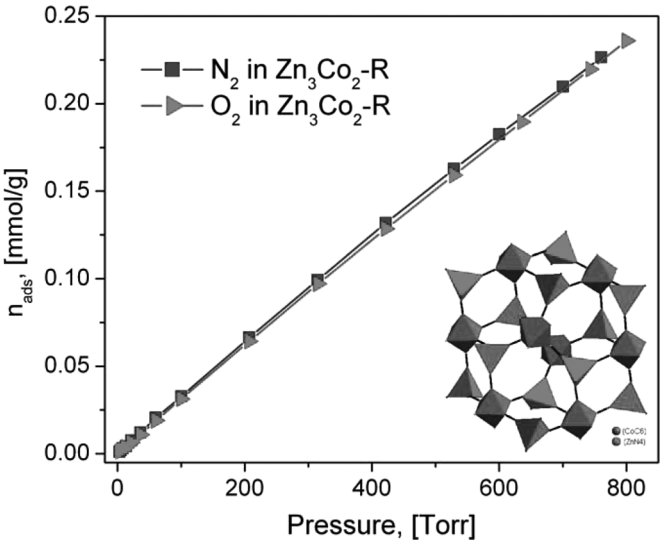

FIG. 5. Nitrogen and oxygen adsorption isotherms in the rhombohedral phase of $Zn_3[Co(CN)_6]_2$ at 0°C. Inset: Porous framework of this solid.

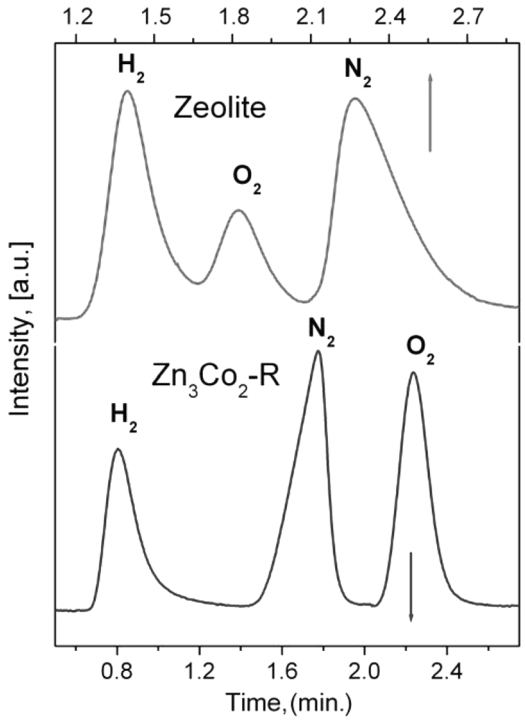

FIG. 6. Chromatographic profiles obtained for the $H_2 + N_2 + O_2$ mixture using columns packed with Zeolite 13X and Zn_3Co_2-R.

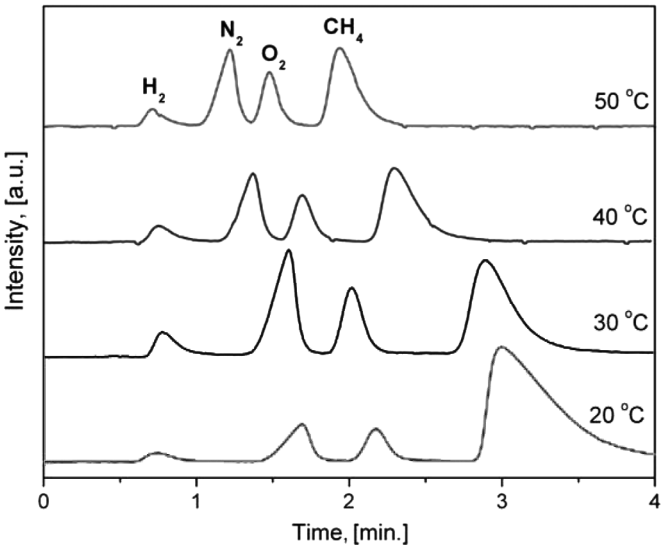

FIG. 7. Chromatographic profiles obtained for the $H_2 + CH_4 + N_2 + O_2$ mixture using the column packed with Zn_3Co_2-R.

nuclear charge (8 versus 7 protons for O and N atoms, respectively) and, in consequence, a more compact electron cloud results. This leads to a smaller molecular size for O_2 (3.46 versus 3.64 Å for N_2 of kinetic diameter) and from this fact to a greater diffusivity through the narrow windows of Zn_3Co_2-R. In the presence of both O_2 and N_2, the entrance of the oxygen molecule into the elliptical cavities is favored and it diffuses through the network of cavities. This leads to a larger retention time for oxygen and explains the observed features for the chromatographic profile obtained for the column packed with Zn_3Co_2-R. This material behaves as a porous carbon for the air separation.

From the observed retention time for hydrogen, also valuable information on the interaction of this molecule with the material packed within the tubing is obtained. The kinetic diameter for H_2 is 2.9 Å, enough small to enable its diffusion through the pore windows of the studied materials. Under the same experimental conditions, the smaller retention time was found for Zn_3Co_2-R (Fig. 6). The porous framework of this material is free of charge centers, and for H_2 the guest-host interaction is dominated by dispersive (van der Waals) type forces (14). The zeolite sample contains exchangeable ions within the channels. These charge centers are able to polarize the electron cloud of the hydrogen molecule, contributing to its stabilization and retention within the cavity. These charge centers are also responsible for a local electric field gradient which interacts with the H_2 quadrupole moment. The existence of these two electrostatic interactions explains the observed greater H_2 retention time for the zeolite packed column.

Figure 7 shows the chromatographic profiles for the mixture of H_2, N_2, O_2, and CH_4 for the Zn_3Co_2-R column at different temperatures. For higher column temperatures, smaller retention times were observed, which is ascribed to a greater diffusion rate for the adsorbates, however, the column continues separating the gases mixture. For that mixture the greatest retention times were observed for methane. Methane has a kinetic diameter of 3.8 Å, enough small to diffuse through the material cavities windows. Such large retention times for methane suggest that this gas could be participating of a relatively strong dispersive guest-host interaction within the cavities. From this evidence a study on the adsorption of light hydrocarbons under equilibrium conditions in porous cyanometallates is now in course.

Figure 8 shows the chromatographic profiles for the $N_2 + O_2$ mixture using columns packed with CoNp and Cd_3Co_2. For these two materials the larger retention times also correspond to O_2 indicating that the N_2 and O_2 separation is related to a kinetic mechanism. The cavities electric field gradient because of the presence of surface metal centers with an unsaturated coordination environment is insufficient to generate a large electrostatic contribution to the adsorption potential. However, compared with Zeolite 13X and Zn_3Co_2-R samples, to obtain well resolved N_2 and O_2 peaks using CoNP and Cd_3Co_2 as column material,

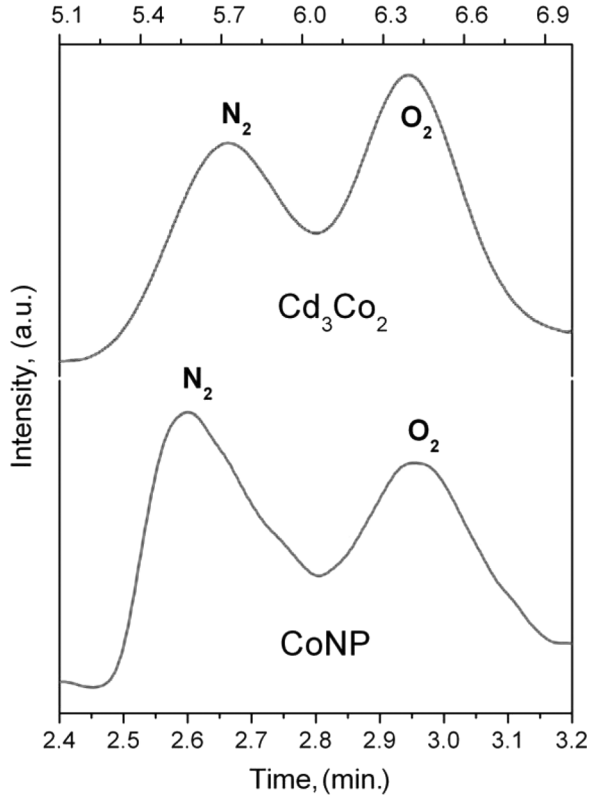

FIG. 8. Chromatographic profiles obtained for the $N_2 + O_2$ mixture using columns packed with CoNP and Cd_3Co_2.

TABLE 2
Experimental data, and net retained volume and calculated adsorption heat values for different gases considered using the Zn_3Co_2-R column

Gas	t_R (min)	t_R (H_2) (min)	t_R (min)	Temp. (K)	V_f (cm^3/min)	V_n (cm^3)	Q_{ads} (KJ/mol)
O_2	1.9	0.86	1	303.15	20	7.3	12.2
O_2	1.7	0.82	0.9	313.15	19.5	6.3	10
O_2	1.6	0.79	0.8	323.15	19.4	5.6	11.1
N_2	1.6	0.9	0.7	303.15	20	5.1	11.2
N_2	1.4	0.8	0.6	313.15	19.5	4.3	9.1
N_2	1.3	0.8	0.5	323.15	19.4	4	10.2
CH_4	2.8	0.9	1.9	303.15	19.4	13.5	19.1
CH_4	2.3	0.8	1.5	313.15	19.4	10.6	15.2
CH_4	2	0.8	1.2	323.15	19.7	8.8	17.2

TABLE 3
Resolution and separator power of the Zn_3Co_2-R column for different binary mixtures at 20°C using Ar as carrier gas

Binary mixture	t_{R1} (min.)	t_{R2} (min.)	w_1 (min.)	w_2 (min.)	Resolution	Separator power
H_2-N_2	1	1.7	0.187	0.173	3.88	2.88
H_2-O_2	1	2.3	0.187	0.15	7.71	6.71
H_2-CH_4	1	3	0.187	0.45	6.27	5.27
N_2-O_2	1.7	2.3	0.173	0.15	3.71	2.71
N_2-CH_4	1.7	3	0.173	0.45	4.17	3.17
O_2-CH_4	2.3	3	0.15	0.45	2.33	1.33

relatively longer columns are required (3.5 m for the profiles shown in Fig. 8). Such behavior is probably related to that electrostatic contribution to the adsorption potential. For CoNp and Cd_3Co_2 the kinetic mechanism dominates but the electrostatic one reduces its separation capability. This is supported by the above discussed results from N_2 and O_2 adsorption under equilibrium conditions.

Of the evaluated porous cyanometallates, the best results for N_2 and O_2 separation were obtained for Zn_3Co_2-R. In Table 2 the collected experimental data and the calculated adsorption heat values for the considered gases using that column material are summarized. At a given temperature, the adsorption heat for O_2 is always greater than for N_2, an expected behavior according to the above discussed results. For methane the adsorption heat values obtained are above 15 kJ/mol, which suggest that this gas could be maintained as adsorbed species in the porous framework of Zn_3Co_2-R even at room temperature, probably through relatively strong dispersive interactions. The cavity region close to the Zn atom has a relatively high electron density which allows the induction of relatively strong instantaneous dipole and quadrupole moments by fluctuations of the involved electron clouds. In Table 3 the calculated separation power for different binary mixtures are reported. For all the mixtures evaluated the Zn_3Co_2-R column is able to produce a well components separation.

CONCLUSIONS

The N_2 and O_2 separation in representative compositions of porous cyanometallates was studied from inverse gas chromatography data. For CoNP, Cd_3Co_2 and Zn_3Co_2-R the N_2 and O_2 separation is dominated by a kinetic mechanism related to a greater diffusivity for O_2 through the materials porous framework. In that sense, these materials behave as porous carbons, even for CoNP and Cd_3Co_2. The presence of certain electric field gradient within the cavities for these last two materials is responsible for an electrostatic contribution to the adsorption potential and to reduction for the column separation capability. The higher values for the separation power were obtained for Zn_3Co_2-R which is free of that electrostatic contribution. For $Zn_3K_2Fe_2$ the K^+ ions located close to the cavities windows impede the access of N_2 and O_2 to the porous framework.

ACKNOWLEDGEMENTS

This study was partially supported by the Projects SEP-CONACyT 61–541 and ICyTDF PIFUTP08–158. The authors thank Dr. J. Balmaseda for the access to the ASAP 2020 facility to obtain the N_2 and O_2 adsorption isotherms.

REFERENCES

1. Sircar, S.; Rao, M.B.; Golden, T.C. (1999) Fractionation of air by zeolites. *Stud. Surf. Sci. Catal.*, 120: 395.
2. Ackley, V.M.; Rege, S.U.; Saxena, H. (2003) Application of natural zeolites in the purification and separation of gases. *Microporous Mesoporous Mater.*, 61: 25.
3. Yang, R.T. (2003) *Adsorbents: Fundamentals and Applications*; (Publ. by John Wiley & Sons, Inc.: Hoboken, New Jersey).
4. Lide, D.R. (2004) *Handbook of Chemistry and Physics*; 84th Edition (CRC Press).
5. Li, Q.G.; Govind, R. (1994) Separation of oxygen from air using coordination complexes: a review. *Ind. Eng. Chem. Res.*, 33: 755.
6. Sircar, S.; Golden, T.C.; Rao, M.B. (1996) Activated carbon for gas separation and storage. *Carbon*, 34: 1.
7. Louer, D.; Vargas, R. (1982) Indexation automatique des diagrammes de poudre par dichotomies successives. *J. Appl. Crystallogr.*, 15: 542.
8. Kiselev, A.V.; Yashin, Ya.I. (1967) *Gazo-Adsorbtsionnaya Khromatografiya* (*Gas-Adsorption Chromatography*); Nauka, Moscow.
9. Balmaseda, J.; Reguera, E.; Gómez, A.; Roque, J.; Vazquez, C.; Autie, M. (2003) On the Microporous Nature of Transition Metal Nitroprussides. *J. Phys. Chem. B*, 107: 11360.
10. Roque, J.; Reguera, E.; Balmaseda, J.; Rodríguez-Hernández, J.; Reguera, L.; del Castillo, L.F. (2007) Porous hexacyanocobaltate-s(III): Role of the metal on the framework properties. *Micropor. Mesopor. Mater.*, 103: 57.
11. Rodríguez-Hernández, J.; Reguera, E.; Lima, E.; Balmaseda, J.; Martínez-García, R.; Yee-Madeira, H. (2007) An atypical coordination in hexacyanometallates: Structure and properties of hexagonal zinc phases. *J. Phys. Chem. Solids*, 68: 1630.
12. Krap, C.P.; Zamora, B.; Reguera, L.; Reguera, E. (2009) Stabilization of cubic and rhombohedral phases of zinc hexacyanocobaltate(III). *Micropor. Mesopor. Mater.*, 120: 414.
13. Lima, E.; Balmaseda, J.; Reguera, E. (2007) *Langmuir*, 23: 5752.
14. Reguera, L.; Balmaseda, J.; del Castillo, L.F.; Reguera, E. (2008) Hydrogen Storage in Porous Cyanometalates: Role of the Exchangeable Alkali Metal. *J. Phys. Chem. C*, 112: 5589.
15. Reguera, L.; Balmaseda, J.; Krap, C.P.; Reguera, E. (2008) Hydrogen Storage in Porous Transition Metals Nitroprussides. *J. Phys. Chem. C*, 112: 10490.
16. Reguera, L.; Krap, C.P.; Balmaseda, J.; Reguera, E. (2008) Hydrogen Storage in Copper Prussian Blue Analogues: Evidence of H_2 Coordination to the Copper Atom. *J. Phys. Chem. C*, 112: 15893.
17. Reguera, L.; Balmaseda, J.; Krap, C.P.; Avila, M.; Reguera, E. (2008) Hydrogen Storage in Zeolite-Like Hexacyanometallates: Role of the Building Block. *J. Phys. Chem. C*, 112: 17443.